Radiotherapy and Oncology 109 (2013) 344–349

Contents lists available at ScienceDirect

Radiotherapy and Oncology

journal homepage: www.thegreenjournal.com

Varian Award paper

Treatment simulations with a statistical deformable motion model to evaluate margins for multiple targets in radiotherapy for high-risk prostate cancer

Sara Thörnqvist [a,b,*], Liv B. Hysing [c], Andras G. Zolnay [d], Matthias Söhn [e], Mischa S. Hoogeman [d], Ludvig P. Muren [a,b,c], Lise Bentzen [b], Ben J.M. Heijmen [d]

[a] Department of Medical Physics; [b] Department of Oncology, Aarhus University Hospital, Denmark; [c] Department of Medical Physics, University of Bergen/Haukeland University Hospital, Norway; [d] Department of Radiation Oncology, Erasmus MC-Daniel den Hoed Cancer Center, Rotterdam, The Netherlands; [e] Department of Radiation Oncology, University Hospital Grosshadern, LMU München, Germany

ARTICLE INFO

Article history:
Received 7 January 2013
Received in revised form 30 August 2013
Accepted 20 September 2013
Available online 31 October 2013

Keywords:
Seminal vesicles
Pelvic lymph nodes
Margin expansion
Statistical deformable motion model
PCA

ABSTRACT

Background and purpose: Deformation and correlated target motion remain challenges for margin recipes in radiotherapy (RT). This study presents a statistical deformable motion model for multiple targets and applies it to margin evaluations for locally advanced prostate cancer i.e. RT of the prostate (CTV-p), seminal vesicles (CTV-sv) and pelvic lymph nodes (CTV-ln).
Material and methods: The 19 patients included in this study, all had 7–10 repeat CT-scans available that were rigidly aligned with the planning CT-scan using intra-prostatic implanted markers, followed by deformable registrations. The displacement vectors from the deformable registrations were used to create patient-specific statistical motion models. The models were applied in treatment simulations to determine probabilities for adequate target coverage, e.g. by establishing distributions of the accumulated dose to 99% of the target volumes (D_{99}) for various CTV–PTV expansions in the planning-CTs.
Results: The method allowed for estimation of the expected accumulated dose and its variance of different DVH parameters for each patient. Simulations of inter-fractional motion resulted in 7, 10, and 18 patients with an average D_{99} >95% of the prescribed dose for CTV-p expansions of 3 mm, 4 mm and 5 mm, respectively. For CTV-sv and CTV-ln, expansions of 3 mm, 5 mm and 7 mm resulted in 1, 11 and 15 vs. 8, 18 and 18 patients respectively with an average D_{99} >95% of the prescription.
Conclusions: Treatment simulations of target motion revealed large individual differences in accumulated dose mainly for CTV-sv, demanding the largest margins whereas those required for CTV-p and CTV-ln were comparable.
 Radiotherapy and Oncology 109 (2013) 344–349

For several major tumor sites managed with radiotherapy (RT), treatment of both primary and elective targets is indicated. These treatments may be compounded by independent motion and deformation of the involved targets. Depending on which target is being used for image-guidance, the uncertainties due to the residual, uncorrected motion should be accounted for the appropriate margin forming the planning target volume (PTV) [1,2]. In radiotherapy of locally advanced prostate cancer – with the prostate as the primary target (CTV-p), and the elective targets consisting of the seminal vesicles (CTV-sv) and the pelvic lymph nodes (CTV-ln) – the different motion patterns present a considerable challenge. The motion of the pelvic lymph nodes is assumed to be rigid since the lymph nodes are closely related to vascular and bony anatomy, but therefore move uncorrelated to the prostate [1,8–9]. In contrary, the motion of the seminal vesicles includes deformations but to what extent the motion is correlated to the prostate is still unclear [4–7]. Consequently, if assumptions regarding this correlation need to be made beforehand in a motion model, they can be unreliable.

Although data supporting deformable target motion exist, most studies addressing the dosimetric effects of residual motion of the pelvic lymph nodes and/or seminal vesicles have simulated the target movement as translational shifts of the planned dose distribution [6,10–13]. Instead, in this paper we propose a statistical method for treatment simulation involving a deformable motion model. The method has been introduced to RT by Söhn et al. [14–15] but so far not been employed for margin evaluations. As the method requires point correspondence we used a data set consisting of repeat CT scans with target delineations, and where these delineations were co-registered with a validated algorithm for non-rigid motion. From the data of voxel displacements, interpolation and extrapolation of the observed (input) target shapes can be made

* Corresponding author. Address: Department of Medical Physics, Aarhus University Hospital, Nørrebrogade 44, Building 5, DK-8000 Aarhus C, Denmark.
E-mail address: sarathoe@rm.dk (S. Thörnqvist).

0167-8140/$ - see front matter © 2013 Elsevier Ireland Ltd. All rights reserved.
http://dx.doi.org/10.1016/j.radonc.2013.09.012

to construct new target shapes according to their probability of occurring. No assumptions of which of the motion patterns that are most prominent need to be made beforehand as it was explicitly handled in the model. The purpose of the study was therefore to introduce the model of residual target motion still present after image guidance on intra-prostatic markers and apply it for dosimetric evaluation of margins for the multiple targets in RT of locally advanced prostate cancer.

Materials and methods

Patients

Nineteen patients with locally advanced prostate cancer previously treated with intensity-modulated RT (IMRT) were included in the study [16]. Each patient had an image set consisting of a planning CT as well as 7–10 additional CT scans acquired evenly distributed throughout their treatment course. All scans were obtained with a slice thickness of 2–3 mm, covering L4 to the anus and with the patient in supine position using a similar fixation device as during RT delivery. The patients had three fiducial gold markers implanted in the prostate, which were used for image guidance. For the planning CT, all but one patient were given contrast to the bladder for the purpose of better distinguishing the bladder wall from the prostate gland. During the course of treatment no bladder or rectum preparation protocol was followed.

For each CT scan the three clinical target volumes: CTV-p, CTV-sv and CTV-ln were delineated by an experienced radiation oncologist [17]; CTV-ln delineations followed the RTOG guidelines [9] except for the pre-sacral nodes which were omitted. In order to secure consistent delineations, all patients were considered as high risk patients T3a and all target segmentations for one patient were performed in a short time interval (usually within one day). Further details about these delineations can be found in Thornqvist et al. [17].

Generation of individualized statistical target motion models

The target delineations in the repeat CT scans were used to construct statistical deformable motion models. Our study evaluated the geometric uncertainties when setup was based on the intra-prostatic fiducial makers. Consequently, all displacements, rigid as well as non-rigid, were derived relative to the fiducial markers. This choice of setup (e.g. instead of bony anatomy) was motivated by previous studies [2,18] but a model could also have been established from setup based on bony anatomy or soft-tissue registrations.

For the common reference system of the fiducial markers in each patient, points on all target surfaces in every CT were distributed with an isotropic resolution of 1 mm. This resulted in target shape vectors, $\boldsymbol{p}$ consisting of N points, varying between 1500 and 229,700 depending on the size of the target. The residual target motion after image guidance on fiducial markers was obtained by calculating the point correspondence between the target shape vectors in the repeat CTs as compared to the planning CT. This was conducted using an in-house developed framework for non-rigid registrations [19–20]. In short, the framework used an inverse-consistent version of the symmetric Thin-Plate Spline Robust-Point Matching (TPS-RPM) algorithm [19–20], where the point correspondence was modeled by soft-assignment, i.e. x points can correspond to y points of the deformed shape. Deterministic annealing was used to refine the correspondence and transformation iteratively, so that each new iteration of the annealing cycle allowed the transformation to be more flexible and reduced the fuzziness in the point correspondence [19–20]. The parameters of the TPS-RPM were optimized individually for each of the three targets both for accuracy, comparing the deviations of the target shape vectors of the transformed structures to those manually delineated in all the repeat CTs [19], as well as for inverse consistency. For CTV-p this resulted in an average ± standard deviation of 0.2 ± 0.2 mm and 0.1 ± 0.0 mm for the accuracy and inverse consistency, respectively. For CTV-sv the accuracy and inverse consistency were 0.3 ± 0.5 mm and 0.2 ± 0.2 mm and for CTV-ln 0.3 ± 0.5 mm and 0.3 ± 0.2 mm.

Each registration of target surfaces resulted in 3D transformation vectors for all target points. This residual movement of the target shape vectors described by the deformation vector fields from the TPS-RPM registrations was subsequently analyzed using principal component analysis (PCA). The PCA method can be used for analyzing high dimensional and possibly correlated data [14–15]. The average and the covariance matrix of the target shape vectors were transformed by the PCA into a set of principal components, ordered by their ability to capture and account for the variability of the input data:

$$\boldsymbol{p}_{\text{sim}} = \bar{\boldsymbol{p}} + \sum_{l=1}^{L} c_l \boldsymbol{q}_l \tag{1}$$

where the eigenvectors $\boldsymbol{q}_l$ are normalized orthogonal vectors ordered by the L largest eigenvalues, λ_l. These eigenvalues quantified the variability described by the components, $l = 1...L$. From Eq. (1) new target shapes, $\boldsymbol{p}_{\text{sim}}$ were generated from a linear combination of the average target shape vector and the components, by sampling c_l from a normal distribution with a zero mean and a variance equivalent to λ_l for each component. In this study all L components were used and individual PCA motion models were constructed for each of the three targets (Fig. 1).

Treatment simulations for margin evaluations

Treatment simulations were conducted on dose distributions derived for PTV expansions of the delineated targets in the planning CT. Uniform CTV-to-PTV expansions ranging from 3 mm to 17 mm were analyzed. In the case of overlapping PTVs a union was used to create a new PTV. Synthetic dose distributions were constructed by convolution with a Gaussian kernel of 1.64 multiplied by the penumbra width, σ_{p} [3], set to 5 mm [7,21]. On the dose distribution of the planning CT, d(·), a new target shape was generated from the deformable target motion model (Eq. (1)) for every treatment fraction, k and accumulated into a final treatment dose, D_{treat}:

$$D_{\text{treat}} = \sum_{k=1}^{N_{\text{fx}}} d(\boldsymbol{p}_{\text{sim}_k}) \tag{2}$$

where N_{fx} is the total number of fractions. In addition, treatment simulations accounting for an imperfect setup were also conducted by adding a rigid translational shift to the PCA-generated target shapes. The rigid shifts were sampled from Gaussian distributions with a mean of zero and with a standard deviation σ_{setup}. For the prostate, seminal vesicles and pelvic lymph nodes σ_{setup} = 1.0–1.7 mm was used [22].

For this study the treatment scenario simulated was a dose prescription of 78 Gy to the prostate and 55 Gy to the elective targets delivered in 37 fractions (N_{fx} = 37). As D_{treat} is accumulated from a configuration of N_{fx} different target shapes, other configurations of target shapes would possibly lead to a different value of D_{treat}. Therefore, in order to evaluate the distribution of D_{treat} in e.g. dose volume parameters for each patient, each fractionated course of treatment was run 1000 times using Monte Carlo simulations. Note that the PCA-based simulations allow for point-correspondance when assesing the variability of D_{treat}. In the following we will

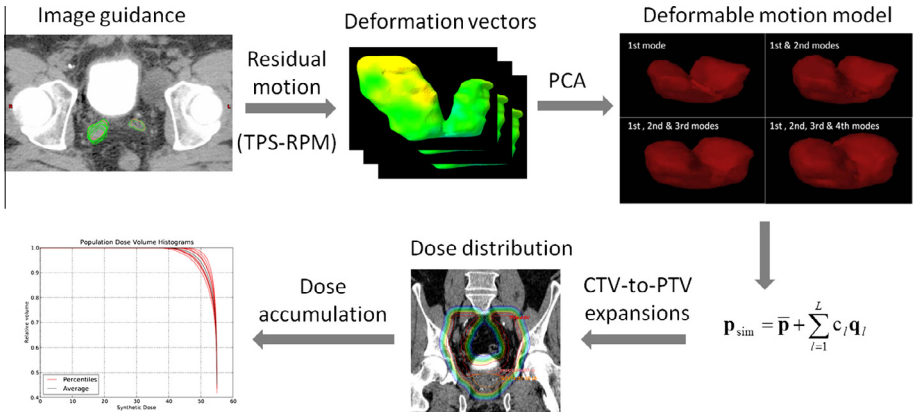

Fig. 1. Schematic presentation of the method of generating new target shapes from variations of the CTVs in the repeat CTs. Here displayed for the seminal vesicles.

present distributions of the dosimetric quantities as averages from the 1000 simulated treatments and the variability of the dosimetric quantities expressed as 10-/90-percentiles.

Results

For all three targets the distribution of the dose to 99% of the target volume (D_{99}) of D_{treat} for CTV-p, CTV-sv and CTV-ln all showed smaller variation as the PTV expansions increased (Fig. 2, Supplementary Fig. S1) expressing increased plan robustness to geometric uncertainties with larger margin size, as expected. In the majority of patients the variations of the distribution of D_{99} exceeded the variations of the distributions of the target volume receiving 95% of the prescribed dose ($V_{95\%}$) (Figs. 2 and 3).

The greatest intra-patient variability of D_{99} was obtained for CTV-sv (Fig. 2). In addition, large inter-patient variations in margin expansions were more frequent for this elective target (Figs. 2 and 3). With a 5 mm CTV-to-PTV margin expansion around CTV-sv nine of the patients had a D_{99} >95% of the prescribed dose in 90% of the simulated treatments with inter-fraction motion (Fig. 2). To further improve coverage for CTV-sv, a margin expansion of at least 9 mm was required for all but three patients to have D_{99} larger than 95% of the prescribed dose in 90% of the treatments for both simulations with and without setup motion. With an 11 mm margin expansion the average D_{99} exceeded 95% of the prescribed dose for all but two patients and to obtain an average D_{99} >95% of the prescription dose in the two remaining patients, a margin expansion of 13 mm was required.

As compared to CTV-sv, CTV-ln displayed a different pattern in both D_{99} and V_{95} of D_{treat} as a function of margin size (Figs. 2 and 3). A 5 mm CTV-to-PTV expansion resulted in all but two of the patients having a D_{99} >95% of the prescribed dose in 90% of the simulated treatments with inter-fraction motion and increasing the margin to 7 mm resulted in 18 of the patients fulfilling this requirement (Fig. 2). To achieve D_{99} >95% of the prescribed dose in 90% of the simulated treatments for all patients, a margin of 15 mm was required.

The impact of setup motion was greatest for the CTV-p resulting in a reduced average D_{99} and V_{95} as well as a wider confidence interval (Supplementary Figs. S1–S2). This difference was most evident when using a CTV-to-PTV margin of 4 mm where including setup motion in the simulations reduced the number of patients having D_{99} >95% of the prescribed dose in 90% of the treatment from 10 to 7 patients (Supplementary Fig. S1). In addition, for simulations including setup motion of CTV-p a large incremental improvement in both D_{99} and $V_{95\%}$ was found when expanding margins from 4 mm to 5 mm; a 4 mm margin in 17 of 19 patients having an average D_{99} larger than 95% of the prescription dose whereas with a 4 mm margin, this criterion was satisfied for only seven patients. Expanding CTV-p by 6 mm resulted in 18 of 19 patients with a D_{99} exceeding 95% of the prescribed dose in 90% of all simulated treatments (Supplementary Fig. S1), irrespective if setup motion was included in the simulations.

Finally, if similar criteria to that used in margin recipes were applied to the result from our treatment simulations e.g. D_{99} >95% of the prescribed dose as well as coverage of the 95% isodose for the

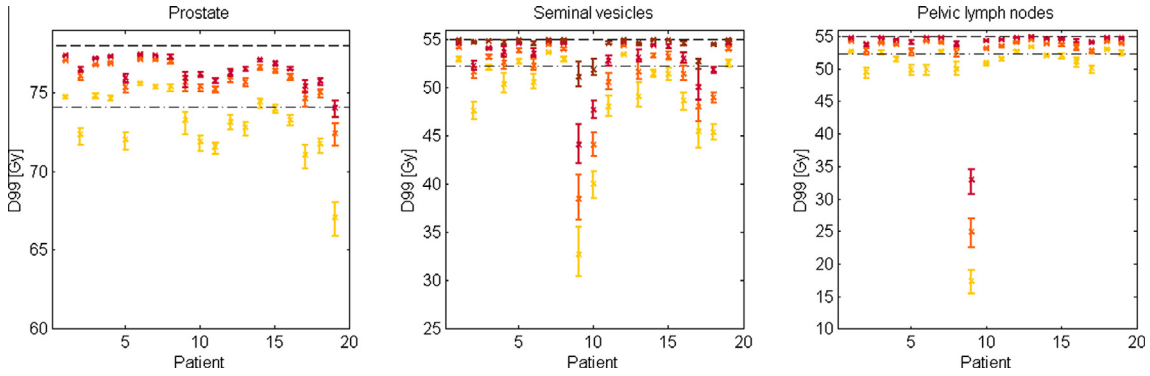

Fig. 2. The distributions of D_{99} from simulations with inter-fraction motion for the prostate CTV (left) and for the seminal vesicle CTV (middle) as well as D_{99} for the pelvic lymph node CTV (right) with varying PTV expansions in color. Yellow denotes 3 mm expansion, orange 5 mm, red 7 mm (6 mm in case of prostate) and an additional 11 mm in brown for the seminal vesicles. Average D_{99} is marked by crosses with 10- and 90-percentiles in bars. Dashed lines denote the prescribed dose and dashed-dotted 95% of the prescription dose. (For interpretation of the reference to colour in this figure legend, the reader is referred to the web version of this article.)

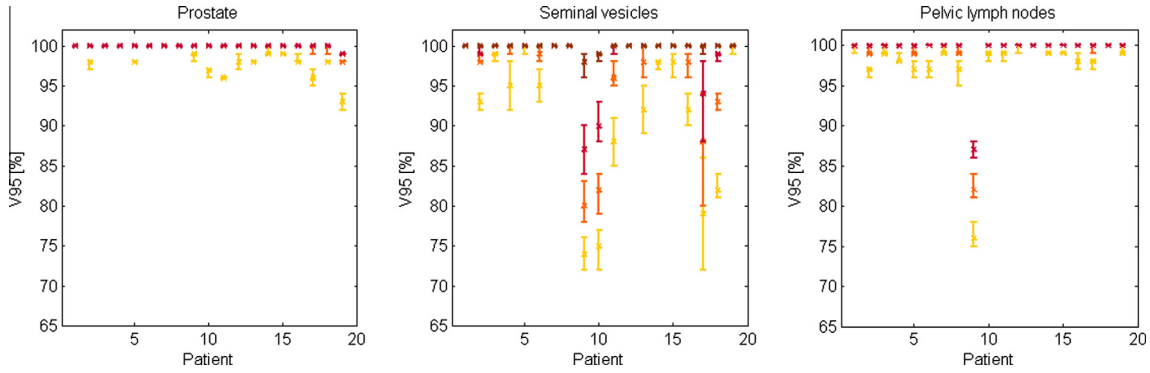

Fig. 3. The distribution of the volume receiving 95% of the prescribed dose ($V_{95\%}$) for simulations with inter-fraction, for prostate CTV (left), seminal vesicles CTV (middle row) and the pelvic lymph node CTV (right) for varying PTV expansions in color. Yellow denotes 3 mm expansion, orange 5 mm, red 7 mm (6 mm in case of prostate) and an additional 11 mm in brown for the seminal vesicles. Average $V_{95\%}$ is marked by crosses with the 10- and 90-percentiles in bars. (For interpretation of the reference to colour in this figure legend, the reader is referred to the web version of this article.)

average treatment in the majority (>89%) of patients, CTV-to-PTV expansions of 5–6 mm for the prostate, 11 mm for the seminal vesicles and 5 mm for the pelvic lymph nodes were needed.

Discussion

In this study we have used a statistical motion model to evaluate margin requirements for the two elective targets, the seminal vesicles and the pelvic lymph nodes and the primary target of the prostate, when IGRT is based on the prostate. Apart from allowing deformations the PCA modeling has other benefits in treatment simulations for margin evaluations.

One benefit was that no prior information about the relative importance of the target motion patterns were needed as this was explicitly part of the PCA. To the best of our knowledge, this study is the first to give CTV-to-PTV margin recommendations from treatment simulations accounting for residual target motion including deformations in male whole pelvic RT. For this treatment, assumptions regarding target motion patterns for individual patients could be error prone as previous studies have revealed large individual differences in motion patterns. Large inter-patient differences were also evident in our dosimetric evalution, especially for CTV-sv (Figs. 2 and 3). Therefore, to account for these variations for the majority of the patients demanded larger margins as compared to both CTV-ln and CTV-p. Acknowledging the deformations of the seminal vesicles and the inadequacy of the conventional margin recipe to account for such motion [3], earlier studies have also applied the deformation vector fields for evaluation of margins [7,23]. Although not including the entire seminal vesicles, Meijer et al. suggested similar margin expansions: 3–6 mm for the prostate and 8 mm for the seminal vesicles [23]. In comparison, our data show that when the entire seminal vesicles were included a 9 mm margin expansion would be adequate, deduced from the distributions of D_{99} as well as V_{95}, for all but three of the patients (Figs. 2 and 3). Investigating margins for the entire seminal vesicles with synthetic dose distributions, as in our approach, Mutanga et al. found 8 mm seminal vesicle margin expansions to be insufficient [7].

Another benefit of the statistical motion model was that in addition to the average accumulated dose to the target we could quantify the variability of this distribution (expressed as 10–90 percentiles) around the average. If the number of inputs available for the patient < the number of fractions, these inputs can be regarded as a sample of each patient's underlying distribution of possible geometries. Consequently, the accumulated target dose (D_{treat}) is also a variable with its own distribution. Our results show that these intra-patient variations were greatest for CTV-sv. As compared to the increase in average D_{99} and V_{95} with increasing margin expansion, the variability had only a slow reduction with larger margin size for the majority of the patients (Figs. 2 and 3). Another study employing treatment simulations of margins for the prostate and the seminal vesicles revealed much larger intra-patient variations in comparison to our results [7]. These discrepancies with the study of Mutanga et al. could also be explained by their low number of samples (i.e. CT scans) which can exaggerate the variance. Especially since this sample was applied to estimate both random and systematic displacements, used independently in their simulations.

In our study we assumed that a sample of 19 patients with their repeat imaging was representative for this group of patients treated with locally advanced prostate cancer. One distinct outlier of the sample (patient 9) was identified, most noticeable for CTV-ln, where even a margin expansion of 9 mm would result in an average D_{99} of 40 Gy, besides leading to the 95% isodose line only covering 91% of the CTV-ln when simulating inter-fraction motion. To increase the coverage of the CTV-ln to 99% would require a margin expansion of 15 mm. This patient also required the largest margins, 13 mm, for full dose coverage of the CTV-sv. The need for these large expansions was explained by a shift of ≈8 mm in the caudal and posterior directions in combination with a rectal gas volume introducing a systematic shift for both the target shapes of the seminal vesicles and the caudal part of the pelvic lymph nodes in the repeat CTs as compared to the planning CT. For such systematic change in anatomy, re-planning instead of applying large margin expansions would probably be more beneficial for the patient. For the prostate, although positioning was based on intra-prostatic fiducial markers, one patient required CTV-to-PTV expansions of 6 mm to achieve an average accumulated dose >95% of the prescribed dose. This patient (patient 19) displayed a consistently larger prostate volume delineated for the repeat CT in comparison to the CTV in the planning CT. Most of the differences were in the cranial part of the prostate which could be caused by differences in location of the CT slices in relation to the anatomy when acquiring the images as well as delineation uncertainties arising from the difficulty in differentiating between bladder wall and prostate base with (planning CT) and without contrast (repeat CTs) injected to the bladder. Indeed, uncertainties in contouring are inevitably introduced when performing manual segmentation of CTVs in a repeat CT-set [24,25]. Motion uncertainties may therefore partly be confounded by uncertainties in delineation in this study, although we did our best to secure consistent target delineations. A PTV should per definition incorporate all uncertainties that can degenerate the intended prescription dose to the targets. However, as our focus was evaluation of margins to compensate residual target motion we opted for reducing the effect of delineation uncertainties by letting the same oncologist delineate the targets for one

patient cohesively in time. It should therefore be noted that as the delineations of the targets all were made by the same radiation oncologist, the modeled margin expansions do not take delineation uncertainties between different radiation oncologists into account. In addition, our margin expansion results for CTV-ln might not be applicable if other delineation guidelines [25] are used. These guidelines were developed to increase consensus following a study revealing large variations in CTV-ln delineations, especially for the pre-sacral nodes (omitted in our study) [26]. For the prostate, reproducibility of delineation has also been studied and shown to be comparable to the smallest direction (left–right) of prostate motion when compared to bony anatomy [27–29]. For the seminal vesicles the motion/deformations have shown to be at least twice as large as the magnitude of the intra-observer delineation variations [5].

The ability of the deformable registration algorithm to accurately calculate the residual motion was another component that influenced the modeling and results. The symmetric TPS-RPM algorithm has previously been validated for pelvic as well as head and neck cancers [19–20]. The evaluation included accuracy (deviations between the transformed and the manually delineated structure), inverse consistency as well as comparison of anatomical landmarks for organs presenting small and large volume changes [19–20]. These studies revealed that even for a highly deformable organ e.g. the bladder and cervix, the majority of the evaluations gave errors less than 5 mm [19–20]. For more rigidly moving organ these numbers were further improved.

The number of repetitions used in the Monte Carlo simulations influences the dosimetric accuracy of our results. Ideally the number of simulations should be as large as feasible in order to minimize the statistical uncertainties. However, our choice reflected a trade-off between minimizing the statistical uncertainties and manageable calculation times; for selected patients we verified that the introduced errors were indeed minimal (data not shown).

Another potential weakness of our study is the modeling of setup motion. Intra-fraction motion has been thoroughly studied for the prostate [22,29–34] but for the two elective targets the data are very limited. We simplified the simulation of setup motion to be a shift, equally probable in all directions and additive to the PCA motion model. This might not be true even for the prostate, where rectum filling has been shown to influence prostate motion [33–34], i.e. not all generated prostate shapes have the same distribution and magnitude of shifts. The strongest impact of the setup motion was observed for the prostate. This was due to the shorter length of the deformation vectors, which on average for the prostate was 2.8 mm as compared to 4.7 mm for the seminal vesicles and 4.4 mm for the pelvic lymph nodes.

Conclusion

In this study we have introduced a statistical deformable motion model to evaluate patient-specific target motion and deformations. Applied on an image material from a series of locally-advanced prostate cancer patients, we found the inter-patient variations to be most pronounced for the CTV-sv. Fulfilling the criteria of D_{99} >95% of the prescribed dose as well as coverage of the 95% isodose for the average treatment in the majority (>89%) of patients, CTV-to-PTV expansions of 5–6 mm for the prostate, 11 mm for the seminal vesicles and 5 mm for the pelvic lymph nodes were found to be required.

Conflict of interest

The authors report no conflict of interest.

Acknowledgement

This work has been supported by research and travel grants from CIRRO – The Lundbeck Foundation Center for Interventional Research in Radiation Oncology.

Appendix A. Supplementary data

Supplementary data associated with this article can be found, in the online version, at http://dx.doi.org/10.1016/j.radonc.2013.09.012.

References

[1] Xia P, Qi P, Hwang A, Kinsey E, Pouliot J, Roach III M. Comparison of three strategies in management of independent movement of the prostate and pelvic lymph nodes. Med Phys 2010;37:5006–13.
[2] Stroom JC, de Boer HCJ, Huizenga H, Visser AG. Inclusion of geometrical uncertainties in radiotherapy treatment planning by means of coverage probability. Int J Radiat Oncol Biol Phys 1999;43:905–19.
[3] Van Herk M, Remeijer P, Rasch C, Lebesque JV. The probability of correct target dosage: dose-population histograms for deriving treatment margins in radiotherapy. Int J Radiat Oncol Biol Phys 2000;47:1121–35.
[4] Smithmans MHP, de Bois J, Sonke JJ, Catton CN, Jaffray DA, Lebesque JV, et al. Residual seminal vesicle displacement in marker-based image-guided radiotherapy for prostate cancer and the impact on margin design. Int J Radiat Oncol Biol Phys 2011;80:590–6.
[5] Van der Wielen G, Mutanga TF, Incrocci L, Kirkels WJ, Vasquez Osorio EM, Hoogeman MS, et al. Deformation of prostate and seminal vesicles relative to intraprostatic fiducial markers. Int J Radiat Oncol Biol Phys 2008;72:1604–11.
[6] Liang J, Wu Q, Yan D. The role of seminal vesicle motion in target margin assessment for online image-guided radiotherapy for prostate cancer. Int J Radiat Oncol Biol Phys 2009;73:935–43.
[7] Mutanga T, de Boer H, van der Wielen G, Hoogeman M, Incrocci L, Heijmen B. Margin evaluation in the presence of deformation, rotation, and translation in prostate and entire seminal vesicle irradiation with daily marker-based setup corrections. Int J Radiat Oncol Biol Phys 2011;81:1160–7.
[8] Shih HA, Harisinghani M, Zietman AL, Wolfgang JA, Saksena M, Weissleder R. Mapping of nodal disease in locally advanced prostate cancer: rethinking the clinical target volume for pelvic nodal irradiation based on vascular rather than bony anatomy. Int J Radiat Oncol Biol Phys 2005;63:1262–9.
[9] Lawton CAF, Michalski J, El-Naqa I, Buyyounouski MK, Lee R, Menard C, et al. RTOG GU radiation oncology specialist reach consensus on pelvic lymph node volumes for high-risk prostate cancer. Int J Radiat Oncol Biol Phys 2009;74:383–7.
[10] Hsu A, Pawlicki T, Luxton G, Hara W, King CR. A study of image-guided intensity-modulated radiotherapy with fiducials for localized prostate cancer including pelvic lymph nodes. Int J Radiat Oncol Biol Phys 2007;68:898–902.
[11] Rossi PJ, Schreibmann E, Jani AB, Master VA, Johnstone PAS. Boost first, eliminate systematic error, and individualize CTV to PTV margin when treating lymph nodes in high-risk prostate cancer. Radiother Oncol 2009;90:353–8.
[12] Mak D, Gill S, Roxby P, Stillie A, Haworth A, Kron T, et al. Seminal vesicle interfraction displacement and margins in image guided radiotherapy for prostate cancer. Radiat Oncol 2012;7:139.
[13] Hwang AB, Chen J, Nguyen TB, Gottschalk AG, Roach III MR, Pouliot J. Irradiation of the prostate and pelvic lymph nodes with an adaptive algorithm. Med Phys 2012;39:1119–24.
[14] Söhn M, Birkner M, Yan D, Alber M. Modelling individual geometric variation based on dominant eigenmodes of organ deformation: implementation and evaluation. Phys Med Biol 2005;50:5893–908.
[15] Söhn M, Sobotta B, Alber M. Dosimetric treatment course simulation based on a statistical model of deformable organ motion. Phys Med Biol 2012;57:3693–709.
[16] Muren LP, Wasbø E, Helle SI, Hysing LB, Karlsdottir A, Odland OH, et al. Intensity-modulated radiotherapy of pelvic lymph nodes in locally advanced prostate cancer: planning procedures and early experiences. Int J Radiat Oncol Biol Phys 2008;71:1034–41.
[17] Thörnqvist S. Petersen J.B.B., Høyer M, Bentzen L, Muren L.P., Propagation of target and organ at risk countours in radiotherapy of prostate cancer using deformable image registration. Acta Oncol 2010;49:1023–32.
[18] Thörnqvist S, Bentzen L, Petersen JBB, Hysing LB, Muren LP. Plan robustness of simultaneous integrated boost radiotherapy of prostate and lymph nodes for different image-guidance and delivery techniques. Acta Oncol 2011;50:926–34.
[19] Vásquez Osorio EM, Hoogeman MS, Bondar L, Levendag PC, Heijmen BJM. A novel flexible framework with automatic feature correspondence optimization for nonrigid registration in radiotherapy. Med Phys 2009;36:2848–59.
[20] Bondar L, Hoogemna MS, Vásquez Osorio EM, Heijmen BJM. A symmetric nonrigid registration method to handle large organ deformations in cervical cancer patients. Med Phys 2010;37:3760–72.

[21] Stroom JC, Storchi PRM. Automatic calculation of three-dimensional margins around treatment volumes in radiotherapy planning. Phys Med Biol 1997;42:745–55.
[22] Poulsen PR, Muren LP, Høyer M. Residual set-up errors in on-line image-guided prostate localization in radiotherapy. Radiother Oncol 2007;85:201–6.
[23] Meijer GJ, de Klerk J, Bzdusek K, van den Berg H, Janssen R, Kaus MR, et al. What CTV-to-PTV margins should be applied for prostate irradiation? Four-dimensional quantitative assessment using model-based deformable image registration techniques. Int J Radiat Oncol Biol Phys 2008;72:1416–25.
[24] de Brabandere M, Hoskin P, Haustermans K, van den Heuvel F, Siebert FA. Prostate post-implant dosimetry: interobserver variability in seed localization, contouring and fusion. Radiother Oncol 2012;104:192–8.
[25] Meijer HJ, Fortuin AA, van Lin EN, Debats OA, Witjes JA, Kaanders JH, et al. Geographical distribution of lymph node metastases on MR lymphography in prostate cancer patients. Radiother Oncol 2013;106:59–63.
[26] Lawton CAF, Michalski J, El-Naqa I, Kuban D, Lee RW, Rostenthal SA, et al. Variation in the definitions of clinical target volumes for pelvic nodal conformal radiation therapy for prostate cancer. Int J Radiat Oncol Biol Phys 2009;74:377–82.
[27] Choi HJ, Kim YS, Lee SH, Park G, Jung JH, Cho BC, et al. Inter- and intra-observer variability in contouring of the prostate gland on planning computed tomography and cone beam computed tomography. Acta Oncol 2011;50:539–46.
[28] Fiorino C, Reni M, Bolognesi A, Cattaneo GM, Calandrino R. Intra- and inter-observer variability in contouring prostate and seminal vesicles: implications for conformal treatment planning. Radiother Oncol 1998;47:285–92.
[29] Zelefsky MJ, Crean D, Mageras GS, Lyas O, Happersett L, Ling CC, et al. Quantification and predictors of prostate position variability in 50 patients evaluated with multiple CT scans during conformal radiotherapy. Radiother Oncol 1999;50:225–34.
[30] Shah AP, Kupelian PA, Willoughby TR, Langen KM, Meeks SL. An evaluation of intrafraction motion of the prostate in the prone and supine positions using electromagnetic tracking. Radiother Oncol 2011;99:37–43.
[31] Budiharto T, Slagmolen P, Haustermans K, Maes F, Junius S, Verstraete J, et al. Intrafractional prostate motion during online image guided intensity-modulated radiotherapy for prostate cancer. Radiother Oncol 2011;98:181–6.
[32] Logadottir A, Korreman S, Petersen PM. Comparison of the accuracy and precision of prostate localization with 2D–2D and 3D images. Radiother Oncol 2011;98:175–80.
[33] Langen KM, Willoughby TR, Meeks SL, Santhanam A, Cunningham A, Levine L, et al. Observations on real-time prostate gland motion using electromagnetic tracking. Int J Radiat Oncol Biol Phys 2008;4:1084–90.
[34] Ghilezan MJ, Jaffray DA, Siewerdsen JH, Van Herk M, Shetty A, Sharpe MB, et al. Prostate gland motion assessed with cine-magnetic resonance imaging (cine-MRI). Int J Radiat Oncol Biol Phys 2005;62:406–17.